United States Patent Application for

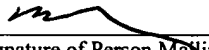**EXTREME CHIRPED/STRETCHED PULSED AMPLIFICATION AND LASER**

Inventors: **PETER J. DELFYETT**
KYUNGBUM KIM
BOJAN RESAN

for the Research Foundation of the University of Central Florida, Incorporated

Attorney's Docket No. UCF-395

EXTREME CHIRPED/STRETCHED PULSED AMPLIFICATION AND LASER

FIELD OF USE

This invention relates to lasers, in particular to methods, devices and systems for

10   generating ultra-short optical pulses with very high power by stretching optical pulses to durations longer than the energy storage time of an optical amplifier, and for deployment of an extreme chirped pulse amplification (XCPA) effect in an laser oscillator and an external amplification.

BACKGROUND AND PRIOR ART

15

Semiconductor gain mediums have a short energy storage lifetime which makes energy extraction from the semiconductor gain medium less efficient compared with other gain mediums that have a longer energy storage lifetime. That is, a semiconductor optical amplifier is easily saturated and, after reaching the saturation regime, energy

20   extraction from the semiconductor optical amplifier is dramatically decreased. It is well known that semiconductor optical amplifiers are not a proper optical amplifier for high power generation.

Previously, external cavity mode-locked semiconductor laser oscillators did not use dispersion management schemes that provide breathing mode operation. In non-

1

breathing modes of operation, laser pulse time duration is similar at all cavity points. However, the preferable pulse duration, prior to a saturable absorber, is much shorter than pulse duration passing through the semiconductor gain media. Short pulses below ~1 ps. bleach the saturable absorber much easier, but such short pulses would initiate different

5   ultra-fast dynamic processes in gain media which are detrimental for the laser operation – the gain would be decreased and the pulse would be strongly nonlinearly chirped. The nonlinear chirp is very difficult to compensate and generate in the end ultrashort pulses

SUMMARY OF THE INVENTION

10   A primary objective of the present invention is to provide methods, devices and systems for generating stretched, linearly chirped optical pulses with high power from the all-semiconductor laser oscillator that could be efficiently externally compressed to approximately 200 fs. This is achieved in the breathing mode operation of laser oscillator by stretching time duration of the pulses passing the gain media, to suppress self-phase

15   modulation, and compressing it subsequently prior to the saturable absorber.

A secondary objective of the present invention is to provide methods, devices and systems for generating ultra-short optical pulses with very high power by increasing the temporal duration of the pulses passing the gain medium to be longer than the storage time of amplifying medium. If the time duration of the optical pulse is longer than the

20   energy storage lifetime, then the energy extraction from semiconductor gain medium is not limited by the energy storage lifetime of the semiconductor optical amplifier but by continuous saturation power multiplied by the time duration of optical pulse. This is done by an extreme chirped pulse amplification technique using chirped fiber Bragg grating.

2

A third objective of the present invention is to provide methods, devices, and systems to deploy an extreme chirped pulse amplification (XCPA) effect in an laser oscillator and to generate extremely linearly chirped high-power pulses externally compressible to approximately 200 fs.

5   Preferred embodiment methods and systems of generating ultrashort optical pulses having increased optical power can include generating optical pulses from a source, such as a modelocked laser source, stretching duration of each of the optical pulses to be greater than energy storage time of an optical amplifier, amplifying the stretched optical pulse with the optical amplifier, and compressing the optical pulse, wherein optical power

10   of the compressed optical pulse can be increased at least approximately 100 times.

The optical pulses can be linear chirped pulses. The mode locked laser source can be a gain-flattened mode-locked laser source, and the optical amplifier can be a semiconductor optical amplifier, such as a grating coupled surface emitting optical amplifier.

15   Preferred embodiments of an extreme chirped pulse amplifier (XCPA), can include methods, systems and devices for generating optical pulses, stretching temporal duration of the optical pulses to be greater than storage time of an amplifying medium, amplifying the stretched optical pulses, and compressing the stretched optical pulse, wherein higher power optical pulses are generated.

20   Additional preferred embodiment methods and systems of generating ultrashort optical pulses having increased optical power can include generating optical pulses with high optical energy and a linear chirp, stretching the duration of each optical pulse to be greater than the energy storage time of an optical amplifier, amplifying the stretched

optical pulse with said optical amplifier, compressing the optical pulse, wherein the optical power of compressed optical pulse is increased.

The embodiments can include modulating the optical pulse whereby the optical pulse is further shortened, by using an active modulator such as a LiNbO3 modulator.

5 Modulating can also include a passive modulator such as a multiple quantum well saturable absorber.

The embodiments can further rout the compressed optical pulse back to the generating step, and output coupling the compressed optical pulse by an fiber coupler.

Additional preferred embodiments of an extreme chirped pulse amplifier (XCPA)

10 laser can include methods, systems and devices for generating optical pulses, stretching temporal duration of the optical pulses to be greater than storage time of an amplifying medium, compressing the stretched optical pulses and amplifying the compressed optical pulses, wherein higher power optical pulses are generated.

The optical pulses can be generated by a gain-flattened mode-locked laser source.

15 Stretching can include a chirped fiber Bragg grating. Compressing can include a dual pass grating compressor.

The embodiments can include modulating the optical pulse wherein the pulse is further shortened, by using an active modulator such as a LiNbO3 modulator. The modulating can also include a passive modulator such as a multiple quantum well

20 saturable absorber.

The optical pulses can be generated by a gain-flattened mode locked laser source, and the stretching and compressing can include a chirped fiber Bragg grating.

Further objects and advantages of this invention will be apparent from the

following detailed description of the presently preferred embodiments which are

illustrated schematically in the accompanying drawings.

5   BRIEF DESCRIPTION OF THE FIGURES

Fig. 1a shows a setup of a preferred embodiment of the extreme chirped pulsed amplifier

invention.

Fig. 1b shows a detail of the optical circulator with arrows indicating the direction of

optical pulse travel.

10   **Fig. 2** is a chart showing the components used for extreme chirped pulse amplification

(XCPA) and the advantage of each for the setup of **Fig. 1a**.

Fig. 3 is a preferred embodiment of the gain-flattened mode-locked laser (GFMLL)

oscillator.

Fig. 4a shows the optical spectrum bandwidth of the GFMLL embodiment of **Fig. 3**

15   operating in active mode-lock at approximately a 200 MHz repetition rate.

Fig. 4b shows the mode-locked output pulse shape in time domain as measured by a fast

photo-detector and digital sampling oscilloscope for **Fig. 3**.

Fig. 5a shows the optical spectrum bandwidth of the GFMLL embodiment operating with

a bandwidth from approximately 970 nm to approximately 980 nm.

20   **Fig. 5b** shows the corresponding mode-locked output pulse shape in time domain as

measured by a fast photo-detector and digital sampling oscilloscope.

Fig. 6a shows the reflection bandwidth for a pair of chirped fiber Bragg grating (CFBG)

used for stretching/compression of the optical pulse.

Fig. 6b shows the group delay for a pair of chirped fiber Bragg grating (CFBG) used for stretching/compression of the optical pulse.

Fig. 7a shows the reflected optical spectrum of the stretched optical pulse after the CFBG that has the positive dispersion **640** as shown in **Fig. 6b**.

Fig. 7b shows the streak camera image of the stretched pulse after the CFBG that has the positive dispersion **640** as shown in **Fig. 6b**.

Fig. 7c shows the reflected optical spectrum of the recompressed pulse after the CFBG that has the negative dispersion **630** as shown in Fig. **6b**.

Fig. 7d shows the streak camera image of the recompressed pulse after the CFBG that has the negative dispersion **630** as shown in Fig. **6b**.

Fig. 8a shows the streak camera image of the output optical pulse train of the GFMLL oscillator.

Fig. 8b shows the streak camera image of the stretched optical pulse.

Fig. 8c shows the streak camera image of the compressed optical pulse.

Fig. 9 shows the normalized optical power spectra at three different points in the extreme chirped pulsed amplifier (X-CPA) invention.

Fig. 10 shows a schematic representation of the GFMLL followed by the preamplifier and pulse picker stage.

Fig. 11a shows the digital sampling oscilloscope image of mode-locked output pulse train of the GFMLL oscillator that operates at 200MHz.

Fig. 11b shows the streak camera image of stretched optical pulse train from the GFMLL oscillator.

Fig. 12a shows the digital sampling oscilloscope image of the mode-locked output pulse after the preamplifier and pulse picker stage in the time domain.

Fig. 12b shows the streak camera image of the output pulse after the preamplifier and pulse picker stage.

Fig. 13 is a schematic representation of the experimental setup to verify the concept of the X-CPA invention using a GFMLL oscillator, optical isolator, and amplifier.

5   **Fig. 14** is a schematic representation of the experimental setup to verify the concept of the X-CPA invention using a GFMLL oscillator, optical isolator, preamplifier, optical isolator, fiber loop as a pulse stretcher, and amplifier.

Fig. 15a shows the optical power spectrum results of the GFMLL used as oscillator in the experimental setup of **Fig. 14**.

10   **Fig. 15b** shows the digital sampling oscilloscope image of GFMLL used as oscillator in the experimental setup of **Figs. 13** and **14**.

Fig. 15c shows the streak camera image of the optical pulse before pulse stretching.

Fig. 15d shows the stream camera image of the optical pulse after pulse stretching using a fiber spool **1445** in **Fig 14**.

15   **Fig. 16a** shows output power vs. input power for an unstretched pulse.

Fig. 16b shows gain vs. output power for an unstretched pulse.

Fig. 17a shows output power vs. input power for a stretched pulse of approximately 3 ns. in time duration.

Fig. 17b shows gain vs. output power for a stretched pulse of approximately 3 ns. in time

20   duration.

Fig. 18a is another schematic representation of the experimental setup to verify the concept of the X-CPA invention.

Fig. 18b shows the chart system parameters and throughputs of the schematic representation of Fig. 18a.

Fig. 19a shows the 100 ns. 10 kHz electrical pulse at the output of the second amplifier 1850.

Fig. 19b shows the signals at the output of the 2nd amplifier, at the output of 2nd plus 1st amplifiers, and at the output of the amplified signal through 2nd and 1st amplifiers

5 amplifier.

Fig. 19c shows the average power vs. peak current for the second amplifier.

Fig. 20a is a schematic representation of another embodiment of experimental setup to verify the concept of the X-CPA invention.

Fig. 20b is a chart showing the system parameters and throughputs of the schematic

10 representation of **Fig. 20a**.

Fig. 20c shows *the optical spectrum of* the amplified signal and the ASE *(Amplified Spontaneous Emission) noise* of the schematic representation of **Fig. 20a**.

Fig. 21 is a simulation sequence flow chart for the preferred embodiment of the invention.

15 **Fig. 22a** shows the simulation results of a 1 nm transform limited (TL'd) pulse without pulse stretching, with 87.5 ps/nm/km CFBG and with 2000 ps/nm/km CFBG.

Fig. 22b shows the simulation results of a 5 nm transform limited (TL'd) pulse without pulse stretching, with 87.5ps/nm/km CFBG and with 2000 ps/nm/km CFBG.

Fig. 23 shows a "Breathing Mode" Mode locked laser (MLL) embodiment with a

20 modulator. The modulator used in Fig. 23 can be a multiple quantum well saturable absorber or a LiNbO3 modulator.

Fig. 24a shows an experimental set-up for dispersion managed semiconductor mode-locked σ-ring cavity laser.

Fig. 24b shows the experimental set-up for diagnostics measurement of spectra and autocorrelation.

Fig. 24c shows the set-up for the dispersion elements and external compressor.

Fig. 25 shows the spectral changes in the laser output after the SA when element 1

5   introduced dispersion is varied and element 2 introduced dispersion is constant.

Fig. 26 shows pulse second harmonic autocorrelation vs. introduced dispersions of the experimental set-up of **Fig. 24a**.

Fig. 27 shows pulse spectrum vs. introduced dispersions by element 1 and element 2 of the experimental set-up of **Fig. 24a**.

10   **Fig. 28** shows the externally compressed autocorrelation and spectral FWHM vs. element 2 introduced dispersions.

Fig. 29a shows the experimental set-up of the hybridly mode-locked σ-cavity semiconductor laser with four outputs for pulse evolution characterization.

Fig. 29b shows the experimental set-up for diagnostics measurement of spectra and

15   autocorrelation.

Figures 30a, 30b, 30c, 30d shows the optical spectra of the experimental set-up of **Fig. 29a**.

Figures 31a, 31b, 31c, 31d shows the cross-correlation traces from the experimental set-up of **Fig. 29a**.

20   **Fig. 32** is a flow diagram representing the algorithm for dispersion-managed mode-locked ring laser simulations.

Fig. 33 is a table of the constants used in the simulations.

Fig. 34 shows the formation of the stretched pulse after the gain media from random noise input.

Fig. 35 shows the mode-locked spectrum build-up after the cavity gain element.

Fig. 36 shows the mode-locked spectrum build-up after the saturable absorber.

Fig. 37a shows the comparison of simulated and measured stretched pulse spectrum after the gain.

5   **Fig. 37b** shows the comparison of simulated and measured compressed pulse spectrum after the saturable absorber.

Fig. 37c shows the comparison of simulated and measured stretched pulse temporal intensity after the gain.

Fig. 37d shows the comparison of simulated and measured compressed pulse temporal

10   intensity after the saturable absorber.

Fig. 38 shows the locking-up of stretched pulses after the gain media to the external-cavity injected Gaussian pulses.

Fig. 39 shows the comparison of the bandwidth-limited calculated and the measured autocorrelations of the externally compressed pulses after the gain media.

15   **Fig. 40** shows the PICASO retrieved temporal intensity and phase of the externally compressed pulses after the gain media.

Fig. 41a shows an experimental setup of dispersion-managed breathing-mode semiconductor mode-locked σ-ring cavity laser with diagnostics.

Fig. 41b shows the spectra of the SOA spontaneous emission, the SA excitonic

20   absorption band, and the mode-locked laser.

Fig. 42a shows the comparison of measured and calculated bandwidth limited pulse autocorrelation.

Fig. 42b shows the measured pulse spectrum with SGH-FROG retrieved spectral phase.

Fig. 43a shows the SHG-FROG experimentally measured trace.

10

Fig. 43b shows the SHG-FROG retrieved trace.

Fig. 44 shows the SHG-FROG retrieved pulse temporal intensity.

DESCRIPTION OF THE PREFERRED EMBODIMENTS

5   Before explaining the disclosed embodiments of the present invention in detail it

is to be understood that the invention is not limited in its application to the details of the

particular arrangements shown since the invention is capable of other embodiments.

Also, the terminology used herein is for the purpose of description and not of limitation.

       Fig. 1a shows a setup of a preferred embodiment of the extreme chirped pulsed

10   amplifier (X-CPA) invention, **100**. Mode-locked laser **110** with semiconductor gain

medium is used as an oscillator. The repetition rate of the oscillator is adjustable.

Optical isolator (OI) **120**, **140** allows the optical pulse to travel in the direction of the

arrow and blocks the optical pulse in the reverse direction. Preamplifier **130** is a

semiconductor optical amplifier that (a) compensates for losses from the first optical

15   isolator **120**, the optical circulator **150**, and the chirped Bragg grating **160**; (b) develops

more power to saturate the amplifier **170**; and (c) adjusts the optical pulse repetition rate.

Optical circulator (OCIR) **150**, **180** is a component that transmits an incoming pulse from

port 1 to port 2 while transmitting a second incoming pulse from port 2 to port 3 as

illustrated by the arrows in **Fig. 1b**. The first chirped fiber Bragg grating (CFBG) **160** is

20   used to stretch the optical pulse and the second chirped fiber Bragg grating (CFBG) **190**

is used to compress the optical pulse. Amplifier **170** is a semiconductor optical amplifier

for high power generation.

       By stretching the time duration of the optical pulse duration such that it is longer

that the energy storage lifetime of the semiconductor gain medium, the energy extraction

11

from the semiconductor gain medium is not limited by the energy storage lifetime of

semiconductor optical amplifier but by continuous saturation power multiplied by the

time duration of optical pulse. In the preferred embodiment, chirped fiber Bragg grating

160, 190 provides dispersion of approximately 2000 ps/nm so that an approximate 8 nm

5   pulse was stretched to approximately 16ns. The recombination lifetime (energy storage

lifetime) of the semiconductor gain medium of amplifier **170** can be less than

approximately 1 ns.

Fig. 2 is a chart showing the preferred components used for chirped pulse

amplification and the advantages as to their use for the setup of **Fig. 1a**.

10

GFMLL Oscillator

Fig. 3 is a preferred embodiment of the oscillator **300** for the X-CPA invention

100. The oscillator is a gain-flattened mode-locked laser (GFMLL) where characteristics

are such that (1) amplitude, phase, and optical spectrum bandwidth can be manipulated

15   using a Fourier plane inside the cavity and (2) active, passive, and hybrid mode-locking

techniques are possible.

The oscillator is comprised of the first high reflector (HR) **305** and second high

reflector **330** that are mirrors that exhibit high reflectance at the operating wavelength of

the oscillator. The band pass filter (BPF) **310** allows the optical spectrum bandwidth of

20   the oscillator output to be changed. The gain flattening filter (GFF) **315** allows the

amplitude of the optical spectrum to be modified. The first lens **320** and the diffraction

grating (DG) **325** form the Fourier plane inside the cavity of oscillator **300**. The second

lens **335** and the third lens **345** collimate the beam to and from the semiconductor optical

amplifier (SOA) **340**. The aperture **350** provides for selection of the spatial beam profile.

The output coupler **360** couples the mode-locked pulse train out from the oscillator. The

fourth lens **355** and the fifth lens **365** provide for stabilization of the cavity.

Fig. 4a shows the optical spectrum bandwidth of the GFMLL oscillator **300** of

Fig. 3 operating in active mode-lock at an approximately 200 MHz repetition rate.

5   Optical bandwidth is approximately 11.4 nm in the range from approximately 961.8 to

approximately 973.2 nm. **Fig. 4b** shows the mode-locked output pulse shape of the

GFMLL oscillator **300** in the time domain as measured by a fast photo-detector and a

digital sampling oscilloscope.

Fig. 5a shows the bandwidth of the GFMLL oscillator **300** of **Fig. 3** with the Fourier

10   plane manipulated to produce optical characteristics different from that of the prior

example. The optical bandwidth is adjusted to approximately 7.8 nm in the range from

approximately 971.1 to approximately 978.9 nm with the optical power spectrum

equalized to an average power of approximately 15.2 mW. Energy per pulse was

approximately 45 pJ. The optical spectrum is adjusted to match the reflection bandwidth

15   of the diffraction grating **325**. **Fig. 5b** shows the mode-locked output pulse shape of the

GFMLL oscillator **300** in the time domain as measured by a fast photo-detector and a

digital sampling oscilloscope. Pulse width is approximately 189 ps.

Active mode-locking for the GFMLL oscillator **300** is achieved by way of gain

modulation. Spectrum modulation is achieved by way of the fourier plane inside the

20   cavity. Homogeneous spectrum narrowing is prevented by using a gain flattening filter.

Stretcher and Compressor

Figs. 6a and **6b** show the reflectance spectrum of the chirped fiber Bragg grating

(CFBG) **160, 190** of **Fig. 1** used for dispersion of the optical pulse. **Fig. 6a** shows the

optical spectrum of the reflection **610** from the first chirped fiber Bragg grating **160** with

a negative dispersion. **Fig. 6a** also shows the optical spectrum of the reflection **620** from

the second chirped fiber Bragg grating **190** with a positive dispersion. The reflectance

bandwidth for both the compressor CFBG **160** and the stretcher CFBG **190** is

5   approximately 8nm in the range from approximately 971nm to approximately 978 nm and

the spectrum exhibits a nice flat reflectance. **Fig. 6b** shows the group delays **630, 640** of

the two CFBG **160, 190** used as a stretcher and a compressor to be approximately 2000

ps/nm each. This means an approximately 8 nm bandwidth optical pulse can be stretched

to approximately 16 ns.

10   **Fig. 7a** shows the reflected optical spectrum for the stretcher CFBG **160** mapped

onto the streak camera image **Fig. 7b** of the optical pulses from the stretcher CFBG **160**.

Fig. 7c shows the reflected optical spectrum for the compressor CFBG **190** mapped onto

the streak camera image **Fig. 7d** of the optical pulses for the compressor CFBG **190**. For

both **Figs. 7c** and **7d**, the vertical axis of the streak camera image represents time and the

15   horizontal axis of the streak camera image represents wavelength. In both images, each

optical pulse has a bandwidth of approximately 8nm and is stretched approximately 16

ns.

        Figs. 8a to **8c** shows streak camera images of the optical pulse at three different

points in the extreme chirped pulsed amplifier (X-CPA) invention, **100**. **Fig. 8a** shows

20   the optical pulse train as output from the oscillator **110**, with an approximately 8nm

optical spectrum bandwidth and a pulse repetition rate of approximately 5 ns. **Fig. 8b**

shows the optical pulse stretched to approximately 16ns from the stretcher CBFG **160**.

Fig. 8c shows the optical pulse compressed from the compressor CBFG **190**. For **Figs.**

8a to 8c, the vertical axis of the streak camera image represents time and the horizontal axis of the streak camera image represents wavelength.

Fig. 9 shows the normalized optical power spectra at three different points in the extreme chirped pulsed amplifier (X-CPA) invention, 100. The optical spectrum 910 is measured at the output of the preamplifier 130, the optical spectrum 920 is measured at the output of the amplifier 170, and the optical spectrum 930 is measured at the output of the compressor CBFG 190. Optical power spectra are nearly flat in all instances.

Preamplifier and Pulse Selection

Fig. 10 shows a schematic representation of the Gain Flattened Mode-Locked Laser 300 followed by the preamplifier and pulse picker 1000. The preamplifier/pulse picker stage is comprised of a first lens 1010, a semiconductor optical amplifier (SOA) 1020, and a second lens 1030. Modulation 1050 of the SOA 1020 provides amplification and pulse selection of the optical pulse train 1040 from the GFMLL 300.

Fig. 11a shows the mode-locked output pulse shape of the GFMLL oscillator 300 in the time domain as measured by a fast photo-detector and a digital sampling oscilloscope. The repetition rate of the oscillator is 200 MHz. Fig. 11b shows a streak camera image (20ns time window) of the stretched pulse from the GFMLL oscillator 300. Fig. 11b has been stretched in the vertical axis to show that optical pulses overlap so that there are approximately four pulses at the same moment as indicated by the horizontal line 1100. Pulse overlap is indicative of inefficient energy sharing between pulses.

Fig. 12a shows the mode-locked output pulse shape after the preamplifier stage 1000 in the time domain as measured by a fast photo-detector and a digital sampling oscilloscope. The output pulse train 1060 of the preamplifier stage 1000 has been

amplified and pulses selected so that the resulting frequency is 50 MHz. **Fig. 12b** shows

a streak camera image (100ns time window) of the stretched pulse from the preamplifier

stage **1000**. Temporal pulse overlap has been eliminated by the pulse biased preamplifier

stage **1000**.

5

Semiconductor Optical Amplifier

The semiconductor optical amplifier of the preamplifier stage **1000** and the

amplifier **170** is an approximately 980nm InGaAs Quantum Well structure that is an

angled stripe inverse bow-tie gain guide amplifier. The angled stripe provides low

10   reflectivity. The structure is a low loss that is good for high power generation and

provides a good spatial mode profile. The amplifier provides large gain volume and

adiabatic beam expansion.

The benefits of using an inverse bow-tie gain guided SOA as the optical gain

element in a high-power external cavity semiconductor laser are further discussed in S.

15   Gee et al., "High-Power Mode-Locked External Cavity Semiconductor Laser Using

Inverse Bow-Tie Semiconductor Optical Amplifiers", *IEEE Journal of Selected Topics in*

Quantum Electronics, Vol. 4, pp 209-215.

Concept Verification

20   Figs. 13 and 14 are schematic representations of the experimental setup to verify

the concept of the X-CPA invention using a semiconductor gain medium. **Fig. 13**

demonstrates the amount of gain saturation without pulse stretching and is comprised of

GFMLL **1310**, optical isolator **1320**, and amplifier **1330**. Amplifier **1330** is further

comprised of the first lens **1340**, the SOA **1350**, and the second lens **1360**.

Fig. 14 demonstrates the amount of gain saturation with pulse stretching and is

comprised of GFMLL **1410**, first optical isolator **1415**, preamplifier **1420**, the second

optical isolator **1440**, optical fiber as an optical pulse stretcher **1445**, and amplifier **1450**.

The preamplifier **1420** is further comprised of the first lens **1425**, the first SOA **1430**, and

5   the second lens **1435**. The amplifier **1450** is further comprised of the third lens **1455**, the

second SOA **1460**, and the fourth lens **1465**.

Figs. 15a through **15d** show the experimental results of the gain saturation of the

experimental setups of **Figs. 13** and **14**. **Fig. 15a** shows the optical power spectrum of

the GFMLL **1410** with FWHM pulse width of approximately 11.4 nm and an average

10   power of approximately 3 mW. **Fig. 15b** shows the mode-locked output pulse shape of

the GFMLL oscillator with pulse duration of approximately 96.4 ps. **Fig. 15c** is a streak

camera image of the pulse at the output of the GFMLL **1410** showing no pulse stretching.

Fig. 15d is a streak camera image of the stretched pulse after fiber spool **1445** that

provides pulse stretching. The pulse is stretched to approximately 2.96ns and

15   corresponds to approximately -64.9 ps/km/nm.

Figs. 16a, 16b, 17a, and **17b** show experimental measurements of gain saturation

determined from the experimental setups of **Figs. 13** and **14**.

Fig. 16a shows output power vs. input power with an unstretched pulse of

approximately 100 ps. The square data points **1610** represent data for an injected current

20   of approximately 250 mA. The circular data points **1620** represent data for an injected

current of approximately 500 mA. The triangular data points **1630** represent data for an

injected current of approximately 750 mA. **Fig. 16b** shows gain vs. input power with an

unstretched pulse of approximately 100 ps. in length. The square data points **1640**

represent data for an injected current of approximately 250 mA. The circular data points

17

1650 represent data for an injected current of approximately 500 mA. The triangular data

points **1660** represent data for an injected current of approximately 750 mA. **Fig. 16b**

shows decreasing gain with output power indicating saturation.

Fig. 17a shows output power vs. input power with a stretched pulse of

5   approximately 3 ns. The square data points **1710** represent data for an injected current of

approximately 250 mA. The circular data points **1720** represent data for an injected

current of approximately 500 mA. The triangular data points **1730** represent data for an

injected current of approximately 750 mA. **Fig. 17b** shows gain vs. input power with a

stretched pulse of approximately 3 ns. in length. The square data points **1740** represent

10   data for an injected current of approximately 250 mA. The circular data points **1750**

represent data for an injected current of approximately 500 mA. The triangular data

points **1760** represent data for an injected current of approximately 750 mA. **Fig. 17b**

shows no saturation behavior of the output power so that energy extraction through the

XCPA will be improved.

15

X-CPA System Experimental Results

Fig. 18a shows a schematic view of the experimental set-up 1800 for the X-CPA

invention. The GFMLL 1810 generates a 200 MHz mode-locked pulse fed to

preamplifier 1815 that amplifies and selects pulses from the optical pulse train so that the

20   output pulse rate is approximately 50 MHz. The optical pulse is stretched by way of the

CFBG 1830 and sent to the amplifier 1845. The optical pulse is further amplified by

amplifier 1845 and sent to a second amplifier 1850. The second amplifier 1850 is pulse

biased with 100ns electrical pulse at 10kHz repetition rate in order to avoid a thermal

management due to high current injection.

Fig. 18b shows the system throughputs at various points around the experimental

setup 1800. At the output of the GFMLL 1810, the optical pulse has energy of

approximately 44 pJ. with a pulse rate of approximately 200 MHz. The preamplifier

1815 provides an increase in pulse energy to approximately 296 pJ. with pulse rate of

5   approximately 50 MHz. After first amplifier 1845, optical pulse energy is approximately

504 pJ. with pulse rate of approximately 50 MHz. The optical pulse energy is further

increase to approximately 11 nJ. and stretched to an approximately 100 ns pulse with

approximately 10 kHz pulse rate by second amplifier 1850.

Fig. 19a shows the approximately 100 ns electrical pulse at approximately 10 kHz

10   pulse rate provided to the second amplifier 1850. **Fig. 19b** shows the amplified

spontaneous emission (ASE) signal 1910 from the first amplifier, the ASE signal 1920

for the first and second amplifiers, and the amplified signal 1930 from the whole system

of **Fig 18a** at the output of the second amplifier 1850. In comparison with the ASE

signal from the first and second amplifiers amplifier 1920, 1930, the dominant amplified

15   signal 1910 due to injection is clearly seen.

Fig. 19c shows the average power 1950 and energy per pulse 1940 vs. peak

current of the device used as second amplifier in the experimental setup 1800. Looking at

the amplified spontaneous emission power in quasi-continuous wave operation, at least

100 nJ. per pulse is obtainable from the experimental set-up 1800.

20

Fig. 20a shows a schematic view of an experimental set-up **2000** for the X-CPA

invention. **Fig 20b** shows the operating parameters for the experimental set-up **2000** of

Fig. 20a. The GFMLL oscillator **2010** generates a 200 MHz mode-locked pulse fed via a

first faraday isolator **2015** to pulse-picker **2020** that selects pulses from the optical pulse

train so that the output pulse rate is approximately 50 MHz and provides approximately

8.4 dB gain. The optical pulse is stretched by way of the CFBG **2030** and provided to

the pre-amplifier **2035**, a RWG SOA, that provides approximately 10.1dB gain. The

optical pulse is passed through the second faraday isolator **2040** and further amplified by

5   the first amplifier **2040** with approximate gain of 9.9 dB, passed through a third faraday

isolator 2050 and provided to a second amplifier **2055**. The second amplifier **2050** is

pulse biased with 100ns electrical pulse at 10kHz repetition rate in order to avoid a

thermal management due to high current injection. Total gain through the system **2000** is

approximately 33.3 dB.

10   **Fig. 20c** shows two optical spectrum curves of final amplifier before and after

signal injection. When a signal is injected into final amplifier, the strong ASE

suppression due to gain saturation is occurred.

15   <u>Simulation Sequence</u>

Fig. 21 is a preferred embodiment of the simulation sequence flow chart for the

invention. **Fig. 21** explains the effect of the X-CPA in terms of stretched pulse widths.

The energy extraction efficiency between unstretched and stretched pulse is simulated

using dynamic semiconductor laser rate equations.

20   For simulation, the oscillator was selected to have parameters of input energy

from approximately 0.1 pJ to approximately 1 nJ and a transform-limited Gaussian input

pulse with an approximately 1nm to approximately 5nm spectrum bandwidth. The

amplifier was selected to have saturation energy of approximately 100 pJ, carrier lifetime

of approximately 200 ps., line-width enhancement factor of approximately 3, and small

25   signal gain of approximately 30 dB. CFBG constants of both approximately 87.5 ps/nm

and approximately 2000 ps/nm dispersion, each with an approximately 1nm and 5nm

optical spectrum bandwidth, were selected for the simulation.

Figures 22a and **22b** are graphs of the simulation results (gain characteristics) of

the invention. The simulation results show how stretching (the basic concept of X-CPA)

5   influences energy extraction efficiency (i.e. extracted gain) in terms of stretched pulse

width.

Fig. 22a shows the simulation results of an approximate 1 nm transform limited

(TL'd) pulse with gain shown on the vertical axis and normalized saturation level

E_{in}/E_{sat} shown on the horizontal axis. The rectangular data points **2310** represent the

10   unstretched pulse. The circular data points **2320** represent the stretched pulse using the

CFBG with an approximately 87.5 ps/nm stretching/compression and approximately 8nm

optical spectrum bandwidth resulting in a pulse length of approximately 87.5 ps. The

triangular circular data points **2330** represent the stretched pulse using the CFBG with

approximately 2000 ps/nm stretching/compression and an approximately 1 nm optical

15   spectrum bandwidth resulting in a pulse length of approximately 2000 ps.

Fig. 22b shows the simulation results of a 5 nm transform limited (TL'd) pulse

with gain shown on the vertical axis and normalized saturation level E_{in}/E_{sat} shown on

the horizontal axis. The rectangular data points **2240** represent the unstretched pulse.

The circular data points **2250** represent the stretched pulse using the CFBG with an

20   approximately 700 ps/nm stretching/compression and approximately 5 nm optical

spectrum bandwidth resulting in a pulse length of approximately 437.5 ps. The triangular

circular data points **2260** represent the stretched pulse using the CFBG with

approximately 2000 ps/nm stretching/compression and an approximately 5 nm optical

spectrum bandwidth resulting in a pulse length of approximately 10,000 ps.

21

The simulation results show the gain difference between a 1 nm and 5 nm

transform-limited pulse laser with the CFBG of approximately 2000 ps/nm

stretching/compression. The simulation results also show that the gain difference

between amplification without and with the CFBG of approximately 2000 ps/nm

5   stretching/compression and approximately 8 nm optical spectrum bandwidth is greater

than approximately 15 dB with approximately 1 nJ input energy for an approximately 5

nm TL'd pulse.

Breathing MLL with Modulator

10   **Fig. 23** shows a <u>compact</u> "Breathing Mode" Mode locked laser (MLL)

embodiment **2300** with a modulator **2350**. The laser is comprised of fiber components

such as the SOA **2310**, the output coupler **2320**, the first optical circulator **2330**, first

CFBG (stretcher) **2380**, the modulator **2350**, the second optical circulator **2370**, and the

second CFBG (compressor) **2340.**

15   Instead of free space bulk diffraction gratings as a pulse stretcher and a pulse

compressor (**Fig. 24**), two CFBGs are put inside cavity to make a laser compact; first

CFBG 2380 is a stretcher and second CFBG 2340 is a compressor. The time duration of

stretched pulse before SOA 2310 is much longer than energy storage time of SOA 2310.

Therefore nonlinearity i.e. self phase modulation which can distort an optical pulse can be

20   reduced and at the same time optical pulse can extract more energy that stored energy

inside SOA 2310. After SOA 2310, optical pulse is divided by output coupler 2320. an

optical pulse which remains inside cavity is compressed by a CFBG stretcher 2340 and

then it goes though a modulator 2350 that has a short gating time. The modulator 2350

can be a passive MQW SA or LiNbO3 intensity modulator.

Dispersion-Managed Breathing Mode-Locked Semiconductor Ring Laser

Figures **24a to 24c** show an experimental set-up **2400** for the dispersion managed breathing-mode σ-ring cavity diode laser. **Fig. 24a** shows the mode-locked

5   semiconductor σ-ring cavity **2402**. **Fig. 24b** shows the set-up for diagnostics measurement of spectra and autocorrelations **2404**. **Fig. 24c** shows the setup **2450** used for dispersion element 1 (compressor) **2416**, dispersion element 2 (stretcher) **2420**, and the external compressor **2435**.

The salient feature is the incorporation of the compressor **2416** and stretcher **2420**

10   in the sigma cavity. An optical isolator **2413**, such as a commercial product from Electro-Optics Technology with isolation >30dB, permits light propagation only in the counterclockwise direction inside the cavity. Since the saturable absorber (SA) **2428** is designed for normal incidence, σ – shape ring propagation is managed with an optical circulator comprising half-wave plate **2418**, quarter-wave plate **2426**, and a polarizing

15   beam-splitter (PBS) **2419**. **Fig. 24c** shows the external compressor **2435**, dispersion element 1, **2416**, and dispersion element 2, **2420** are standard dual pass grating compressors **2451, 2454**, (we used commercial Spectrogon gratings with 1800 lines per mm), with internal telescopes, hence they can operate as pulse compressors or stretchers. The introduced dispersion amounts of those components were controlled by the relative

20   position between gratings. Output ports **2414, 2424** are after the gain medium **2410** and after the SA **2428**. Both intracavity diode **2410** and external cavity semiconductor optical amplifier (SOA) **2432** are angle-stripe, approximately 0.5 mm long SOAs. The chirped SA **2428** has multiple quantum wells with thickness of approximately 70/75/80 Å to sustain broad bandwidth saturable absorption. Passive mode locking is established using

23

the SA **2428** and a dc-biased (approximately 190 mA) intracavity SOA **2410**. The sigma

cavity laser outputs **2415, 2425** are individually directed to a spectrometer **2430**, such as a

commercial Jarell Ash equipped with a Reticon CCD camera, or to an external SOA **2432**

to boost the power prior to the autocorrelator **2436**, such as a commercial Femtocrome

5   FR-103.

The pulse train repetition rate is approximately 1.116 GHz, corresponding to the

31st harmonic of the laser cavity. The pulse spectrum after the SA **2428** is recorded from

output **2425** while keeping the introduced dispersion by element 2 **2420** constant and

varying the dispersion introduced by element 1 **2416** and is shown in **Fig. 25**. A fixed

10   dispersion of approximately 4.57 ps/nm is introduced by element 2 **2420**. In each

dispersion element, a 1 cm grating position variation corresponds to an introduced

dispersion of approximately 0.83 ps/nm. There is an optimal grating position in element

1 **2416**, which introduces approximately –0.25 ps/nm additional dispersion than that

introduced by element 2 **2420**. When such optimal dispersion is introduced, the obtained

15   spectrum is the broadest and pulses are compressible to their shortest duration. The

optimal total dispersion of approximately –0.25 ps/nm introduced by elements 1 **2416** and

2 **2420** compensates the dispersion of other cavity elements. Small variations in the total

cavity dispersion cause dramatic changes in the spectral shape and width.

Fig. 26 displays measurements after the gain element **2410** from output 1 **2415** of

20   the second harmonic intensity autocorrelation versus dispersion introduced by elements 1

2416 and 2 **2420**. Data points are collected for movable grating position adjustments of

approximately 1 cm yielding approximately 200 data points and the map is obtained by

interpolation. On-diagonal map values occur for dispersions of equal magnitude and

opposite sign in elements 1 **2416** and 2 **2420**. From the map we can see that when the

24

laser operates in the regime near the diagonal region of the map, output pulses were

shorter without coherent spikes. In contrast, noise bursts – temporally broad pulses with

coherence spikes - were observed for off-diagonal map values.

Fig. 27 illustrates similar measurement after the SA **2428** from output 2 **2425** of

5   spectral bandwidth (FWHM) versus dispersion in elements 1 **2416** and 2 **2420**. The

bandwidth is slightly broader close to the map diagonal. The results along the diagonal of

the map are summarized in **Fig. 28**. Externally compressed pulse autocorrelation and

bandwidth are plotted versus dispersion introduced by element 2 **2420**. A threshold value

for the dispersion occurs at approximately –3.3 and approximately +3.3 ps/nm for

10   dispersion elements 1 **2416** and 2 **2420**, respectively. Beyond this threshold, the spectrum

broadens more than twice, output pulses are externally compressible below approximately

1 ps and the laser is operating in breathing mode. The breathing mode means that with

each cavity round-trip, the pulse is stretched when passing through the gain medium **2410**

and compressed when incident on the SA **2428**.

15   **Figures 29a** and **29b** show a cross-correlation measurement set-up. **Fig. 29a**

shows a hybridly mode-locked σ-cavity laser **2902** with four outputs **2915, 2922, 2930,**

2932, for pulse evolution characterization. **Fig. 29b** shows the set-up **2904** for

measurements of spectra as well as autocorrelation and cross-correlation traces. The

intracavity SOA **2910** was biased with approximately 92 mA of DC and a superimposed

20   radio frequency (RF) signal modulated the gain at approximately 323 MHz. Introduced

dispersions were approximately -5 ps/nm in the element 1 (compressor) **2916** and

approximately +5 ps/nm in element 2 (stretcher) **2930**. As depicted in **Fig. 29b**, the

signals from the four different cavity ports **2940** are split after the SOA amplifier **2943**

with a 50/50 beam splitter **2946**. Half of the beam is guided through the delay line **2950**

and then recombined with the other half which passes through the external compressor

2947. The pulse from the cavity is combined with a compressed version of itself, and the

autocorrelator **2960** signal reveals the two-pulse autocorrelation trace. The side pulse on

the trace represents the cross-correlation of the two versions of the pulse. When the

5   compressed version is much shorter than the original (in this case it is more than

approximately 40 times shorter), the cross-correlation trace measures the temporal profile

of original pulse intensity.

        Figures 30a, 30b, 30c, 30d shows the optical power spectra from the four key

points of the cavity – after the gain media (intracavity SOA) output **2915**, before the SA

10   output **2930**, after the SA output **2932**, and before entering back to the gain media output

2922. Spectra of the pulse propagating through the laser cavity are similar in shape, with

the peak around the same wavelength.

        Figures 31a, 31b, 31c, 31d shows the cross-correlation traces from the four laser

cavity outputs. The stretched pulses exhibit an asymmetric temporal profile with a steep

15   leading edge and a long decaying trailing edge. The stretched pulse traces Fig. 31a and

Fig. 31d also contain an artifact from the autocorrelation. The dashed line depicts how

the contributions from autocorrelation and the cross-correlation overlap. The cross-

correlation traces from before and after the SA in Fig. 31b and Fig. 31c are similar to

autocorrelation traces, since those are already short pulses in the cavity and were not

20   externally compressible. The stretched pulse before and after the gain media is more than

approximately 20 times broader than compressed one before and after the SA. This

measured pulse duration change while propagating in the cavity demonstrates that laser

operates in the breathing mode. The pulse energy after the cavity gain media is more than

approximately 100 times higher than before the gain media as shown in Fig. 31a and Fig. 31d. This verifies that intracavity chirped pulse amplification was achieved.

Dispersion-Managed Breathing Mode-Locked Semiconductor Ring Laser Numerical

5   Simulation

            Fig. 32 is a flow diagram representing the algorithm to simulate the laser pulse

formation from random noise input in the dispersion-managed breathing mode-locked

semiconductor ring laser of **Fig. 24a**. Elements of the Split-Step Fourier algorithm are

arranged in an order analogous to the semiconductor ring laser. The constants used in the

10   simulations are listed in the table of **Fig. 33**. A frequency filter with FWHM equal to

approximately 7.6 nm accounts for the finite bandwidth of the SA and the semiconductor

gain. A time filter with FWHM equal to approximately 131 ps. represents a RF

modulation of the SOA as a gain element. The results from the simulations are scaled to

the measured pulse energies after the cavity gain element energy is equal to

15   approximately 33 pJ and after the SA energy is equal to 0.86 pJ. The pulse energy after

the gain is approximately 1.64 times larger than the gain saturation energy and the pulse

energy after the SA is approximately 2.8 times larger than the saturation energy of the

SA.

            The mode-locked stretched pulse formation from input random noise is shown in

20   **Fig. 34**. The steady-state pulse shape is formed after approximately 350 cavity round

trips.

            Figures 35 and **36** show the build-up of the mode-locked spectra after the cavity

gain element and after the SA. The steady-state pulse spectral and temporal intensity

after approximately 600 simulated cavity round trips are compared with the measured

ones as shown in **Figures 37a, 37b, 37c and 37d**. The main part of the simulated stretch

pulse fit well as compared to the experimentally measured pulse. The leading part of the

cross-correlation trace of **Fig. 37c** contains an artifact from the middle autocorrelation

trace of **Fig. 31a** which enhances the leading and trailing edge of the pulse measured by

5   the two-pulse autocorrelation technique.

In **Fig. 37d** the steady-state simulated compressed pulse temporal intensity after

the SA is compared with the corresponding pulse retrieved by the PICASO method. The

pulse temporal intensity and phase are calculated by use of the PICASO algorithm from

the measure spectrum and second-order intensity autocorrelation. Both pulses exhibit the

10   same trend. The difference between the retrieved pulse by PICASO and the pulse

obtained through simulation differs by approximately 150 fs. This difference may be due

to additional dispersion encountered in the experimental setup prior to the intensity

correlation measurements, minor inaccuracies in the PICASO algorithm, or the finite

resolution of the temporal grid used in the simulation.

15   **Fig. 38** shows simulation of lock-up of the dispersion-managed breathing-mode

semiconductor mode-locked ring laser to externally injected Gaussian pulses. Lock-up is

achieved after less than approximately 50 cavity round trips.

Fig. 39 shows a comparison of the measured and the Fourier limited calculated

second-harmonic autocorrelation of externally compressed pulses from the experimental

20   set-up of **Fig. 29a**. The set-up **2904** for measurements of spectra as well as

autocorrelation and cross-correlation traces is used without the delay line **2950** in the

diagnostics part. Linearly-chirped pulses from the laser output **2915** after the cavity gain

media **2910** are compressed using a dual-grating external cavity compressor **2947**. The

bandwidth-limited autocorrelation is calculated from the measured spectrum of the laser

output after the gain element as in (a) of Fig. 30. The calculated autocorrelation FWHM

of approximately 404 fs. is only approximately 10% shorter than the measured FWHM of

approximately 445 fs. From this, we can conclude that efficient intracavity linear

chirping and amplification as well as external cavity amplification and compression are

5   achieved.

Fig. 40 shows the pulse temporal intensity and phase retrieved by the PICASO

algorithm. The pulses from the output after the gain medium are externally compressed

to FWHM of approximately 274 fs. A measured average amplified power of

approximately 6.25 mW after external compression at the repetition rate of approximately

10   323 MHz would correspond to pulse energy of approximately 19 pJ with peak power

approximately 70W and a focused intensity of approximately 1 GW/cm^2.

SHG-FROG Experimental Results

Fig. 41a shows an experimental setup of dispersion-managed breathing-mode

15   semiconductor mode-locked σ-ring cavity laser with diagnostics. As in the embodiment

of Fig. 24a, the salient feature of the laser cavity is the incorporation of dispersion

element 1 4110 and dispersion element 2 4120. The elements1 4110 and 2 4120 as well

as the external compressor 4130 are typical dual pass grating compressors with internal

telescopes providing tunable positive or negative group velocity dispersion (GVD).

20   The laser output after the cavity gain element is externally amplified and

characterized by a spectrometer 4160, a second-harmonic intensity autocorrelator 4140,

and second-harmonic generation frequency-resolved optical grating (SHG-FROG) 4150.

Pulse retrieval is performed with commercial software such as Femtosoft Technologies

utilizing a standard SHG-FROG set-up.

The SOAs **4170, 4180** used have a gain peak that is red shifted with respect to the excitonic saturable absorption band. The mode-locked spectrum is located between the gain peak and excitonic absorption band as shown in **Fig. 41b**. In this wavelength configuration, for up-chirped pulses the red spectral part of the pulse is strongly

5   amplified. Since for up-chirped pulses the red part of the pulse arrives first to the SOA **4170**, due to gain depletion the leading (red) part is strongly amplified in temporal domain. The combination of these temporal and spectral effects tends to amplify only the red portion of the pulse and therefore limits the mode-locked spectral width. The laser output spectrum was no broader than approximately 4 nm for the up-chirped pulses. For

10   down-chirped pulses the amplification in the spectral and temporal domain can be balanced. The red part of the pulse is strongly amplified due to red shifted gain peak, but the blue part of the pulse is first incident to the SOA **4170** and is amplified more before the SOA **4170** gain depletes. It should be noted that up chirping would be preferable if the SOA **4170** gain peak is blue shifted with respect to the excitonic absorption peak.

15   **Figs. 42a** and **42b** show the measured laser output after external cavity amplification and compression. As displayed in Fig. **42a**, the measured autocorrelation **4210** of FWHM equal to approximately 310 fs, is 1.7 times wider than the bandwidth limited autocorrelation **4220**, calculated from the measured spectrum shown in Fig. **42b**. **Fig. 42b** additionally shows the broadened pulse spectrum **4230** of FWHM equal to

20   approximately 9 nm using down chirping along with the corresponding SHG-FROG retrieved spectral phase **4240**.

        Fig. 43a shows the SHG-FROG experimentally measured trace and **Fig. 43b** shows the SHG-FROG retrieved trace. This demonstrates that the retrieved trace recovers the salient features observed in the experimentally generated trace. The

extracted temporal intensity profile along with corresponding phase plots are shown in

Fig. 44. The retrieved pulse FWHM is approximately 185 fs.

The invention encompasses a wide body of disciplines ranging from astrophysics

to nuclear physics with applications ranging from communications to medical surgery.

5   The invention has applications in the medical sciences. The X-CPA laser

becomes a very accurate scalpel in the performance of femtosecond precision surgery.

Ultra-short pulsed lasers allow for non-thermal laser tissue interaction and small

collateral tissue damage as compared to longer-pulsed lasers. Cutting by photo-

disruption produces much less damage to surrounding tissues than photo-ablation. Intra-

10   ocular microsurgery can ablate or vaporize tissue without creating large "shock waves"

that can damage surrounding healthy tissue.

The invention has application in surgery such as ophthalmic surgery, photo-

refractive surgery, glaucoma treatment, and corneal refractive surgery to correct refractive

problems such as nearsightedness and astigmatism. Surgical procedures such as laser

15   channel cuts for intra-corneal ring segment (ICRS) implantation, femtosecond lamellar

keratoplasty (FLK), and intrastromal vision correction, that rely on ultra-short pulsed

lasers, are in development. Additionally, the invention can be used for photodynamic

therapy of various carcinomas, for hard tissue ablation in dental procedures, and for

multiple surgical procedures that have heretofore been performed with a surgical scalpel

20   or a longer-pulsed laser.

The invention can be used for high-speed diagnostic applications such as multi-

photon imaging, optical coherence tomography (OCT), and terahertz imaging. The

invention can be used to measure optical-matter phenomena in condensed matter

materials, to measure very fast events, processes, mechanisms, interactions, and the like.

Such applications are useful not only for medical diagnosis, but also in the study of chemical reactions at the atomic and molecular level.

The invention has applications in the material sciences. Ultra-short pulsed lasers can be used for material processing by way of non-thermal ablation and deposition of

5   materials.

The invention has applications for commercial information networks, along with military and aerospace optical signal processing systems. In communications, the invention can be used as a high-speed transmitter of optical data in fiber optic networks.

In computers, the invention can be used as a transmitter of optical data, as high

10   speed processors of optical data, and as high speed switches of optical data, and the like.

Additionally the invention can be used in the communication through free space.

While the invention has been described, disclosed, illustrated and shown in various terms of certain embodiments or modifications which it has presumed in practice, the scope of the invention is not intended to be, nor should it be deemed to be, limited

15   thereby and such other modifications or embodiments as may be suggested by the teachings herein are particularly reserved especially as they fall within the breadth and scope of the claims here appended.